SECOND EUROPEAN CONFERENCE ON EARTHQUAKE ENGINEERING
AND SEISMOLOGY, ISTANBUL AUG. 25-29, 2014

EFFET OF LOADING HISTORY ON FRAGİLİTY CURVES OF REİNFORCED CONCRETE BRIDGE PIERS UNDER MULTIDIRECTIONAL LOADING

Fouad KEHILA[1] Mustapha REMKI[2] Hakim BECHTOULA[3] Youcef MEHANI[4] and Abderrahmane KIBBOUA[5]

ABSTRACT

Damage to reinforced concrete bridge piers was and still an important topic for many researchers. Although numerous promising damage indices have been formulated, relatively a few attempts have been made to calibrate them against the observed damage either from earthquake or laboratory tests. Understanding the parameters controlling the damage progress during an earthquake is an important issue to should be solved. In this study, an assessment procedure is presented for the seismic performance of reinforced concrete, RC, bridge piers through fragility curves. Four square reinforced concrete bridge piers were tested under axial load and reversed cycling horizontal load in order to investigate the strength, stiffness, and energy dissipation of reinforced concrete bridge piers. A computer program SeismoStruct, was used to analyze the tested specimens.
Damage indices aim to provide a means of quantifying numerically the performance level in reinforced concrete bridge piers sustained under earthquake loading.
Damage progress was assessed using Park and Ang damage index defined for five damage ranks. Combining the damage indices for the different cycles, the fragility curves for the four RC bridge piers were derived assuming a lognormal distribution.

INTRODUCTION

In past earthquakes, including the 1995 Kobe earthquake, 1999 Chi-Chi earthquake and 2008 Wenchuan earthquake, a large number of bridges were severely damaged as a result of a failure of the RC (reinforced concrete) bridge piers.

Some investigations have been carried out in the past to investigate the inelastic behavior of Reinforced Concrete Bridge piers (Chang 2010; Han et al. 2013) subjected to strong earthquakes, and specimens simulating reinforced concrete bridge piers have been tested under various loading conditions such as static and dynamic cyclic loading.

Sheikh tested fifty-six bar specimens under monotonic loading and used the results of experimental testing (Sheikh, 1978) to present a numerical procedure for predicting the behavior of plastic hinge.

[1] MSc, National Earthquake Engineering Research Center- CGS, Algiers, fouad.kehila@gmail.com
[2] MSc, National Earthquake Engineering Research Center- CGS, Algiers, musremki@gmail.com
[3] Dr, National Earthquake Engineering Research Center- CGS, Algiers, bechhakim@gmail.com
[4] Dr, National Earthquake Engineering Research Center- CGS, Algiers, mehani_youcef@yahoo.com
[5] Dr, National Earthquake Engineering Research Center- CGS, Algiers, a_kibboua@yahoo.com

In a study by Cheok and Stone (Cheok and Stone 1990), six circular concrete bridge columns of scale 1:6 were subjected to quasi-static cyclic loading to study their behavior while varying some of their parameters such as the aspect ratio, axial load, and the type of material.

Some researchers have undertaken full-scale dynamic testing of bridges but mainly limited to ambient vibration testing and/or forced vibration testing using external exciters for the purpose of determining the natural periods, modal shapes and modal damping ratios (Salawu and Williams, 1993).

Sheikh and Toklucu tested twenty-seven reinforced concrete columns under monotonic axial compression (Sheikh and Toklucu, 1993). In this study, they investigated the effect of various parameters such as the amount and type of lateral steel, spacing of lateral steel and specimen size.

Twelve circular concrete bridge columns of scale 1:4 were tested under cyclic loading. (El-Bahy A., Kunnath, Stone, and Taylor, 1999). The purpose of this testing was to study the cumulative damage in concrete bridge piers designed with AASHTO specifications. The researchers have also conducted a study of the effect of variable amplitude loading on the column response. (El-Bahy, Kunnath, Stone, and Taylor, 1999).

In Japan, Kawashima and others have tested around 50 concrete bridge columns using quasi-static methods. The purpose of testing has been related to various objectives such as the effect of loading hysteresis on ductility, effect of interlocking ties on strength and ductility, verifying plastic hinge lengths, etc. (Takemura & Kawashima, 1997; Kawashima, Shoji, and Sakakibara, 2000; Fujikura, Kawashima, Shoji, Zhang, and Takemura, 2000).

Another series of bridge column testing was done in which two prototype and four models were subjected to quasi-static testing (Yeh, Mo, and Yang, 2002).

Full-scale testing of five concrete bridge columns was undertaken by Bae (Bae and Bayrak, 2008) to study their seismic performance. Bae and Bayrak performed cyclic testing under constant axial load.

Two large-scale tests on bridges on shake tables were conducted for verification of bridge condition assessment (Chen, Feng, and Soyoz, 2008). One test was on a two-column reinforced bridge bent and other was on a three-column bent.

In order to investigate the seismic performance of RC bridge piers with different design detailing and different horizontal loading histories and axial load intensities, four reversed cyclic static tests of cantilever piers was conducted.

Hereafter, the four specimens are called tp031, tp032, tp033 and tp034. Geometrical characteristics and reinforcement detailing of specimens, are summarized in Table 1. The specimens were selected from the data bank of Sakai and Kawashima (2002).

1. TEST DESIGN

1.1. Specimen design

Four specimens called tp031, tp032, tp033 and tp034 were designed and tested, columns are 1.35 m tall (effective height) and have a section of 400 mm x 400 mm, twenty D13 bars and D6 bars with an interval of 50 mm is provided for longitudinal and tie bars, respectively. The yield strength of D13 and D6 bars are 374 MPa and 363 MPa, respectively. The longitudinal reinforcement ratio and the volumetric tie reinforcement ratio are 1.58% and 0.79%, respectively. The concrete strength is between 22.9 and 23.0 MPa.

The layouts of the dimensions, reinforcements of the test specimens were shown in Fig. 1, Fig. 2 and Table.1.

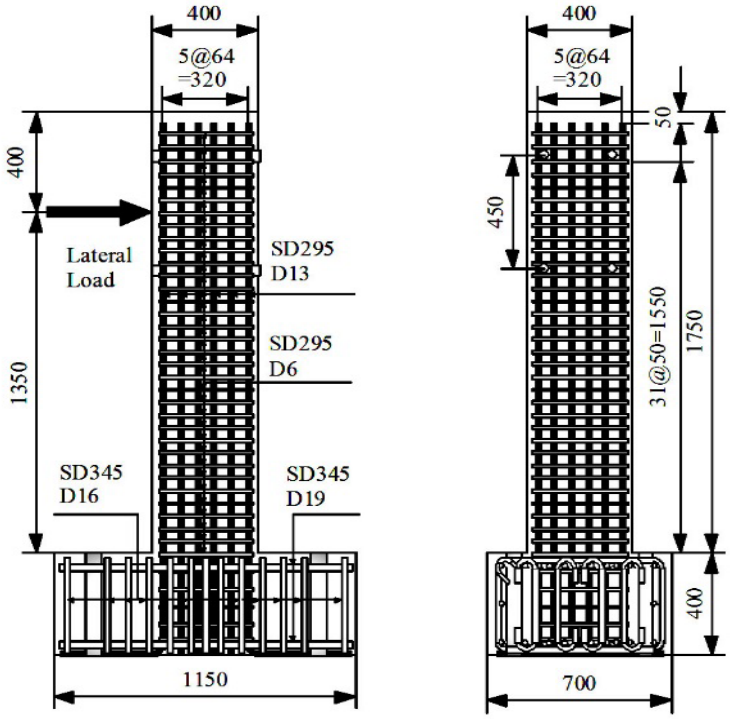

Figure 1. Geometrical characteristics of specimen's

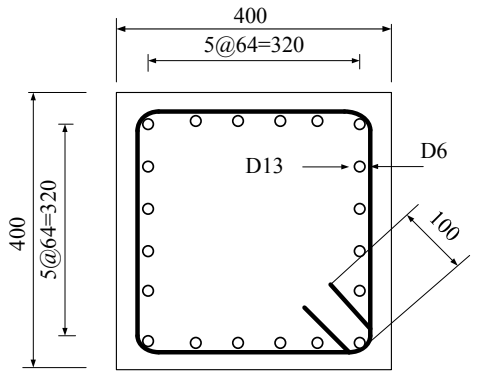

Figure 2. Cross-section (mm)

Table 1. Properties of tested specimens

Item	tp031	tp032	tp033	tp034
Section size (mm) Effective height (mm) / Effective depth (mm) Longitudinal reinforcement ratio %	400×400 (square) 1350 / 360 1.58			
Cylinder strength of concrete (MPa)	22.9	23.0	22.9	23.0
Longitudinal reinforcement (yield strength)	SD295 D13 (374MPa)			
Tie reinforcement (yield strength)	SD295 D6 (363MPa)			
Axial Force (kN)	470	-170	-10~310	-170~420

1.2. Loading history

Fig.3 show the cyclic loading history used for specimens tp031 to tp034, the bridge piers stepwise loaded in the lateral direction under four different vertical loads: (tp031) constant compression axial load corresponding to normalized axial load ($N/f'_c\ A_g$) of 12.8%; (tp032) constant tension axial load corresponding to -4.6 % of the normalized axial load; (tp033) varying axial load

corresponding to -0.3% to 8.5% normalized axial load; and for (tp034) a varying axial load corresponding to -4.6% to 11.4% normalized axial load. The lateral displacement was stepwise increased such as 0.5%, 1%, 1.5% drift, until failure, with three load reversals cycles that were applied per step.

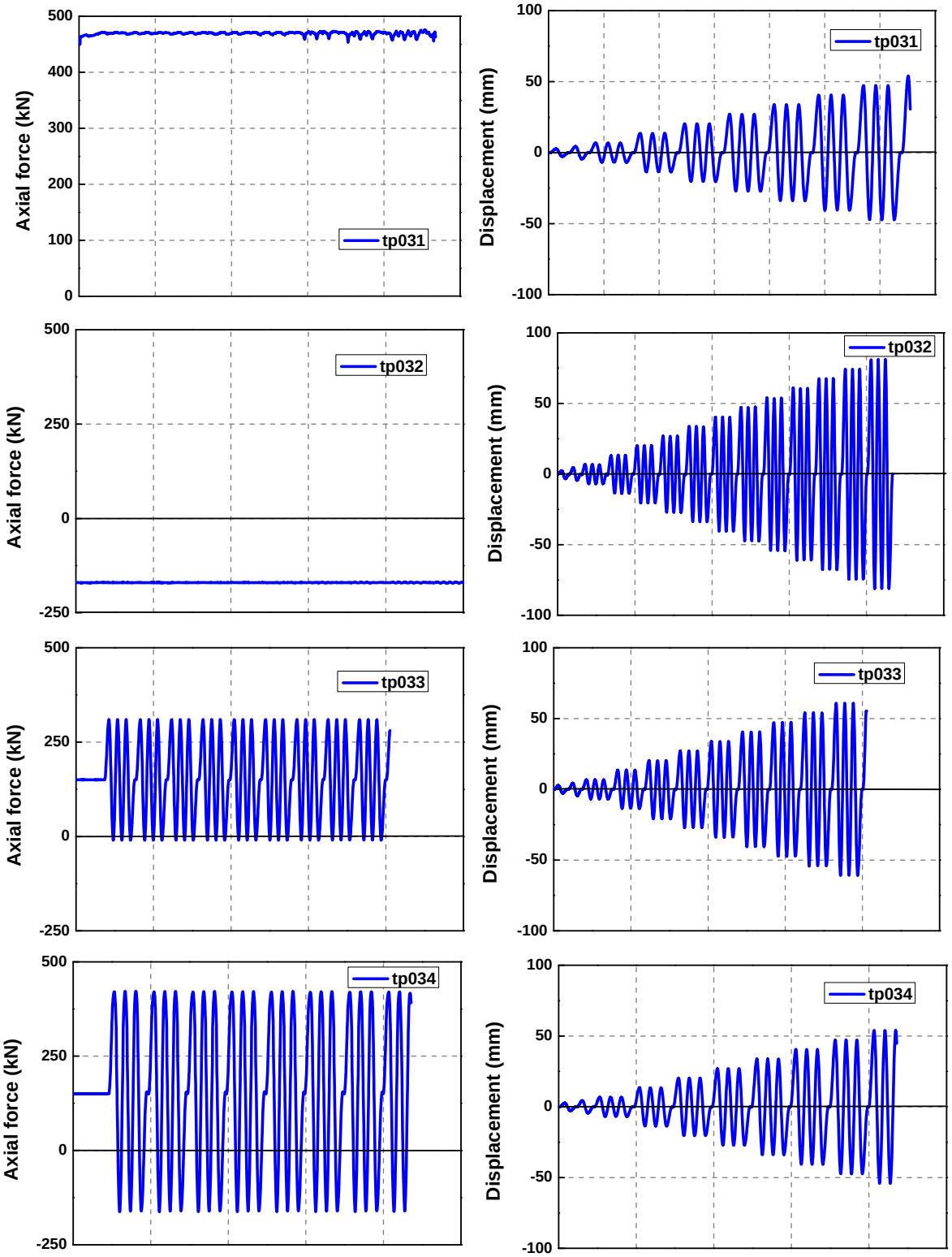

Figure 3. Loading condition for specimen tp031~ tp033

2. TEST RESULTS

2.1. Failure mode

From the observation of Fig.4, displacement represents the displacement toward C direction, where compression due to the vertical load increases in tp033 and tp034. In the tp031 specimen, the flexural strength is 174kN and 161kN in the positive and negative displacements, respectively. On the other hand, strength of tp032 specimen is only 97kN and 92kN in positive and negative displacements, respectively, which are nearly 55% on the flexural strength of tp031 specimen. As described above, the shear movement occurs along shear cracks, but this does not necessarily results in a significant deterioration of lateral restoring force. The lateral restoring force starts to deteriorate at 3.5-4% drift when covering concrete start to spall off. At 4.5% drift, the restoring force reduced to 50% of the maximum values, and the loading terminated at 6% drift since a longitudinal bar ruptured. At this stage, not only the covering concrete but also the core concrete suffered extensive failure at nearly 40% of its total sectional area. Among 20 longitudinal bars, one ruptured and 19 bars buckled in complicated modes. It is noted that a sudden deteriorate of lateral restoring force resulted from shear failure did not take place until the end of the loading.

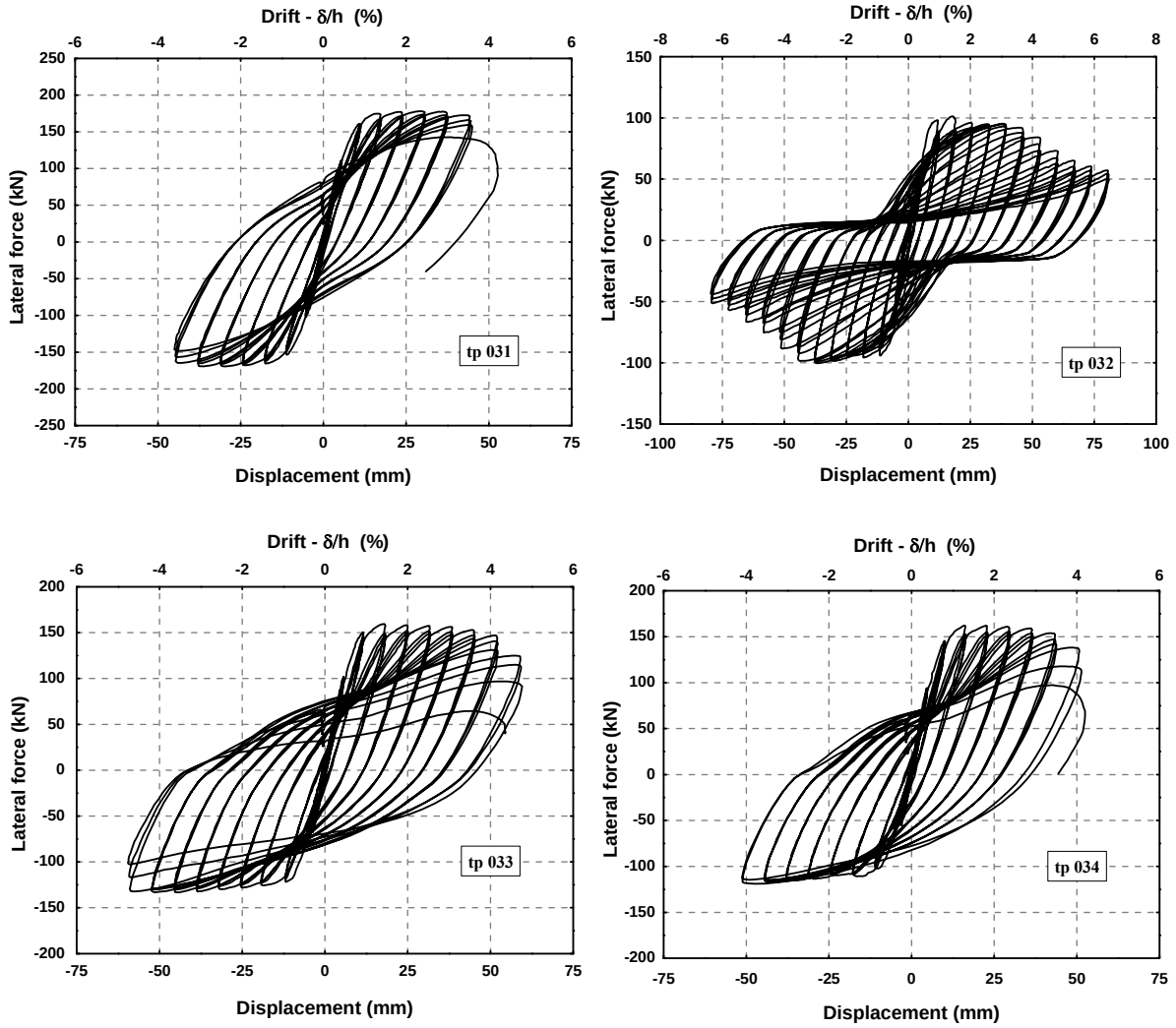

Figure 4. Hysteresis loops of the lateral force vs. lateral displacement relations

2.2. Envelope of a cyclic load-displacement curves

Table.2 summarizes the displacement ductility, $\mu_\Delta=\Delta_u/\Delta_y$, of the piers using the load displacement curves in Fig.4. The yield displacement Δ_y was defined as the displacement of the intersection point of the following two lines, the straight line that passes through the origin and $0.75V_{max}$ of the envelope curve, and the straight line that passes through V_{max} on the envelope curve and is parallel to the x-axis. The ultimate displacement Δ_u was defined as the displacement that occurs when the strength of the descending branch of the force displacement envelope curve becomes less than $0.85V_{max}$, as shown in Fig.5.

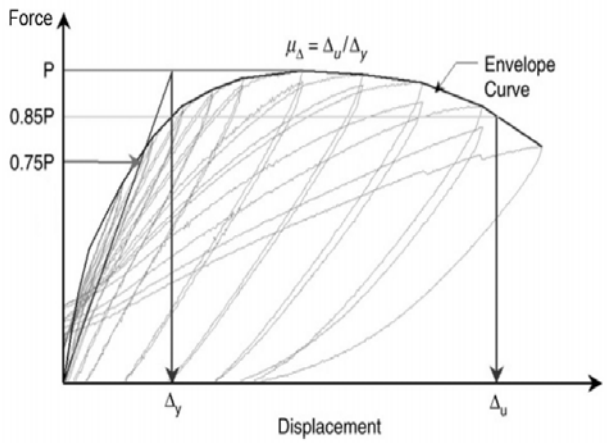

Figure 5. Definition of displacement ductility

Fig.6 presents the envelop curves of the RC pier specimens. The tp031 specimen with positive constant axial load showed the worst seismic behavior. The tp032 specimens showed relatively ductile behavior after reaching their ultimate load.

The strength decay after reaching the maximum loading at around 2.0% drift level can be evaluated from Fig.6. The tp032 specimen had higher displacement amplitude showed 50% strength decay at a drift level of 3.0% while the tp033 and tp034 specimen showed 10% decay at a drift level of 3.0%.

All of the specimens showed that the displacement ductility was greater than 5.

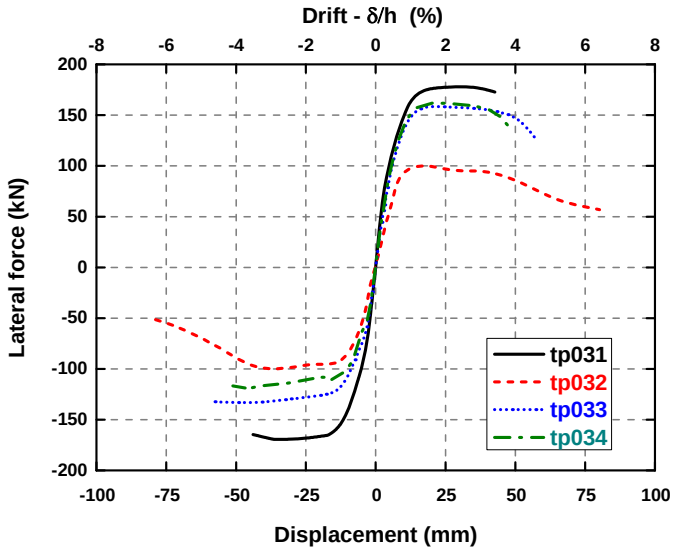

Figure 6. The envelope of cyclic load-displacement curve

The yield force, idealized yield displacement, peak force, ultimate lateral force, ultimate displacement and ductility of envelope curves of specimens were listed in Table.2.

Table 2. Parameters of envelope curve of specimens

Specimen	Yield Force (kN)	Yield Displacement mm)	Ultimate Force (kN)	Ultimate Displacement (mm)	Displacement ductility μ_Δ
tp031	167.48	7.93	177.66	42.66	5.38
tp032	93.17	8.24	93.17	57.54	6.98
tp033	151.49	8.36	151.49	57.75	6.90
tp034	154.77	7.98	154.77	49.03	6.14

2.3. Energy dissipation capacity

The dissipation energy (ΔW_i) in one loop of hysteresis displacement is determined by integrating the area bounded by the hysteresis loop as indicated by Eq.(1). The accumulated dissipation energy (ΔW) in the column specimens is determined by Eq. (2).

$$\Delta W_i = \int_{-u_{max}}^{u_{max}} (F_l(u) - F_{ul}(u))du \quad (1)$$

$$\Delta W = \sum_i \Delta W_i \quad (2)$$

Where $F_l(u)$ and $F_{ul}(u)$ are the forces at displacement, u during loading and unloading process.

In which ΔW is energy dissipation during one reversal and W is an elastic energy as defined in figure 7.

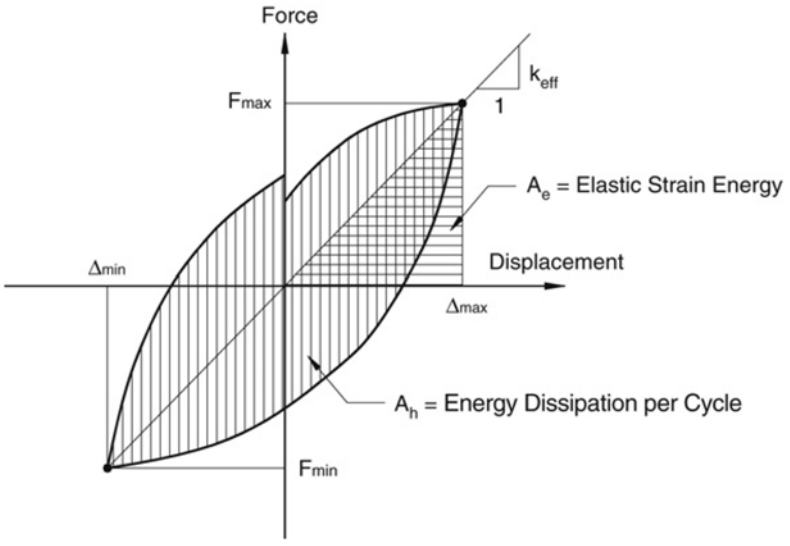

Figure 7. Energy dissipation by hysteresis behavior.

The amount of absorption energy in each load cycle was calculated from the hysteresis loop in Fig.4, and is shown in Fig.8(a) and Fig.8(b) shows comparative curves of the cumulative energy absorption capacity of the piers.

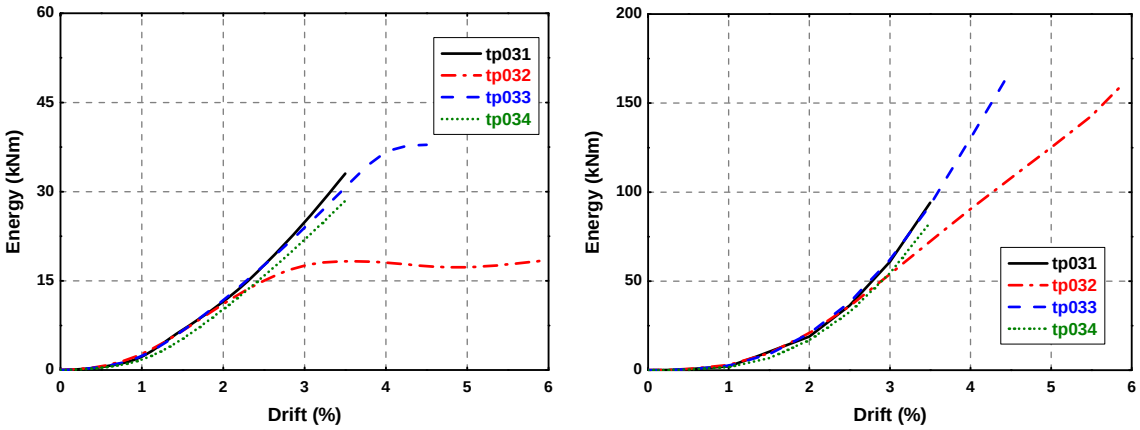

(a) Energy dissipation per cycle (b) Accumulated energy dissipation

Figure 8. Energy dissipation

Fig.8 shows the dissipated energy per cycle and the cumulative dissipated energy of specimen tp031 to tp034. It can be observed through Fig.8(a) that the energy dissipated per cycle for specimen tp032 is constant from 3% to 6% drift, which was not the case for the three other specimens. This is due mainly to the constant axial force that was applied to the specimen, tp032. The amount of energy dissipated per cycle was the same for the four specimens until a drift of 2%. Beyond that a bifurcation is observed, see Fig.8(a). The cumulative dissipated energy is illustrated in Fig.8(b). At 4.5% drift, the cumulative dissipated energy of specimen tp032 was only 65% of that of specimen tp033.

3. NUMERICAL MODELLING

Numerical models were developed and analyzed in SeismoStruct for the same geometrical and loading characteristics of the experimental test tp031 to tp034.

The SeismoStruct is a finite element package capable of predicting the large displacements behaviour of space frames under static or dynamic loading, taking into account geometric nonlinearities and material inelasticity.

Several models are available for concrete and steel materials as well as for the frame elements.

The confined and unconfined concrete is modelled using a unified stress-strain model based on the formulation initially proposed by Mander et al (1988) for a concrete subjected to uniaxial compressive loading and confined by transverse reinforcement. The following mechanical properties are defined in table1 for the four specimens, the strain at peak stress ε_c=0.002, the confinement factor is assumed as 1.2 for confined concrete and as 1 for the unconfined one.

The steel model is based on the stress-strain relationship proposed by Menegotto and Pinto (1973), coupled with the isotropic hardening rules proposed by Filippou *et al* (1983). The steel mechanical properties adopted are those previously presented in Table.1.

3.1. Experimental and numerical comparison

Fig.9 shows a comparison between the experimental and the analytical results in terms of hysteresis loops, lateral force-displacement, or drift, for the tested specimens. As illustrated in the figure, the analytical results show reasonable agreement with the experimental ones. The analysis not only correctly predicted the stiffness, load, and deformation at the peak, but also captured the post-peak softening as well.

The constructed models for specimen tp033 and tp034 captured the effect of the axial load variation on the piers performance. The results show that the compressive axial load in the push direction increased the strength capacity, and that the tensile axial load in the pull direction reduced the strength capacity.

The maximum experimental and analytical horizontal peak loads of the four specimens are summarized in Table.3. In all cases the ratio experimental peak strength to the analytical one

(Q_{exp}/Q_{ana}) was greater than 0.95 except for specimen tp032 in negative side. The mean ratios of experimental-to-analytical maximum peaks were 0.96 with a coefficient of variance (COV) of 1% for the positive side and 0.97 with a coefficient of variance (COV) of 4% for the negative side.

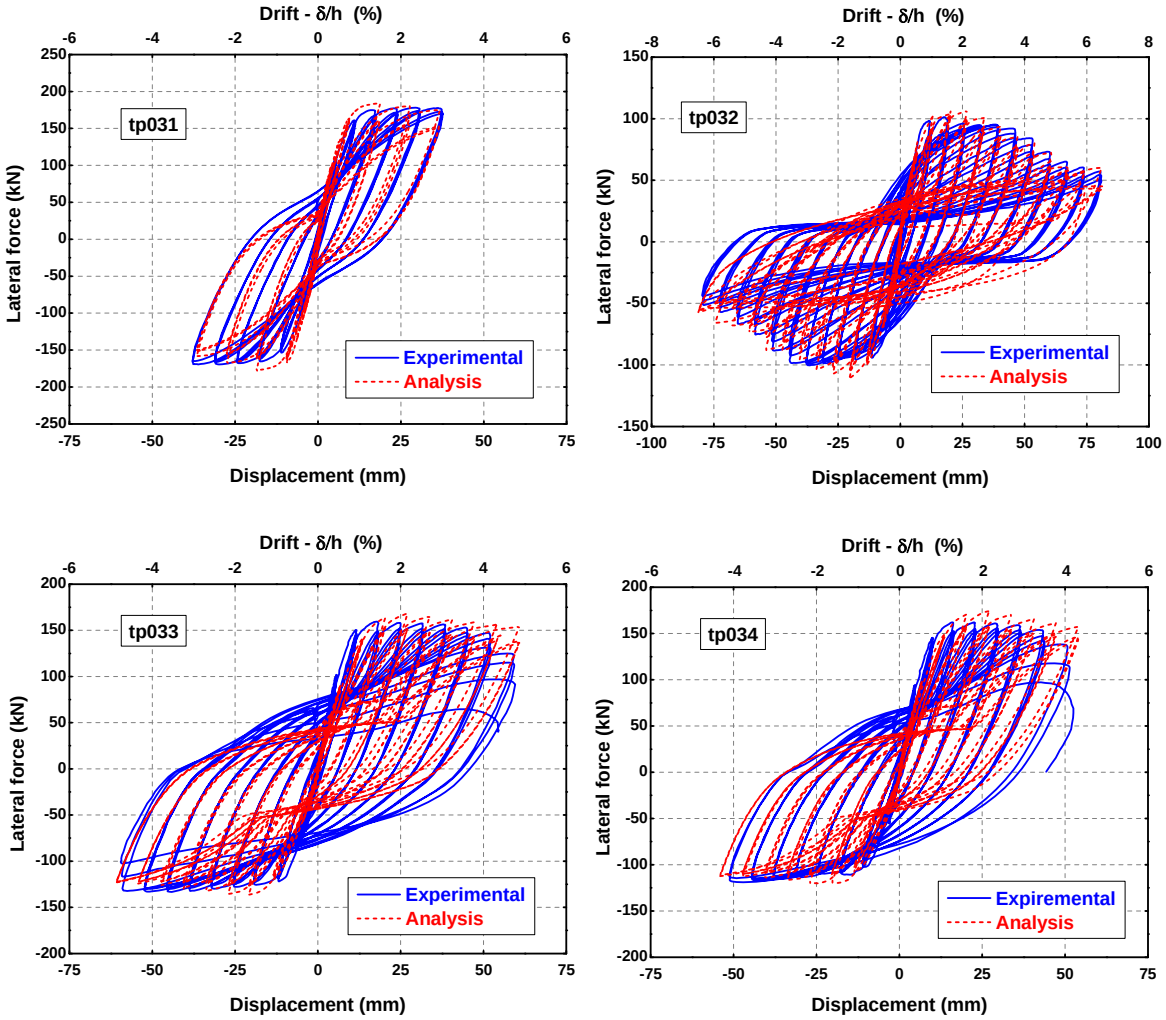

Figure 9. Comparison of results from the experimental results

Table 3. Comparison between the experiment and the analytical peak strengths

Specimen	Positive side			Negative side		
	Experiment	Analysis	Ratio	Experiment	Analysis	Ratio
	Q_{exp} (kN)	Q_{ana} (kN)	(Q_{exp}/Q_{ana})	Q_{exp} (kN)	Q_{ana} (kN)	(Q_{exp}/Q_{ana})
tp031	178.1	184.3	0.97	-169.4	-178.1	0.95
tp032	101.2	106.2	0.95	-100.4	-110.9	0.91
tp033	159.5	168.1	0.95	-133.3	-136.4	0.98
tp034	162.1	170.9	0.95	-119.0	-116.5	1.02
Mean			0.96			0.97
COV			0.01			0.04

4. DAMAGE EVOLUTION

The damage for individual elements is calculated based on element data such as element deformations, forces, or dissipated energy. These engineering parameters must be extracted from the solution and processed for calculating a Damage index. A Damage model is defined as an operator that calculates the Damage index by applying a specific damage rule.

The damage index can be recorded for subsequent loss assessment and in some cases; it may be used by the analysis components for degrading constitutive stiffness or strength parameters.

The combined damage model introduced by Park and Ang (1985) is widely used due to its simplicity and the fact that calibration information is available. Park-Ang is a combined damage model, which was originally calculated for RC components. The Park-Ang model calculates the damage index is a linear combination of the damage caused by excessive deformation, and repeated cyclic loading, captured in the form of dissipated energy. The general form of the Park-Ang damage formulation is as follows Eq.(3):

$$DI = \frac{\delta_{max}}{\delta_u} + \beta \frac{\int dE}{F_y . \delta_u} \tag{3}$$

Where δ_{max} is the maximum displacement of the structural member, δ_u is the ultimate displacement, $\int dE$ is the dissipated hysteretic energy and F_y is the yielding strength of the structural member; β is a degradation parameter which represents the influence of cyclic response on column damage and can be estimated with empirical expressions based on structural parameters.

A detailed classification of damage levels suggested by (Park, Ang and Wen 1985) is used to relate the observed empirical damages and the calculated damage indices.

Table 4. Park-Ang damage level classifications

Damage level	Damage index	Damage measure
I	DI < 0.1	No damage, localized minor cracking
II	0.1 ≤ DI ≤ 0.25	Minor damage, light cracking throughout
III	0.25 ≤ DI ≤ 0.4	Moderate damage, severe cracking, localized spalling
IV	0.4 ≤ DI ≤ 1.0	Severe damage, crushing of cracking, reinforcement exposed
V	DI ≥ 1	Loss of element load resistance

The computed damage to all specimens using Park and Ang models described is shown in Fig. 10. Of all the specimens, Park and Ang model shows little or no damage through the first ten cycles. The Park-Ang model shows a gradual progression of damage throughout the load history with increasing accumulation of damage at each increase in displacement level.

For all specimens, the Park-Ang model provided a very good measure of damage at different limit states.

For the specimen tp032 with constant tension axial load was subjected to a much larger drift amplitude. Failure of the specimen was recorded in less than 30 cycles. The Park-Ang model seems to perform better when the displacement amplitudes are significantly larger than the yield displacement.

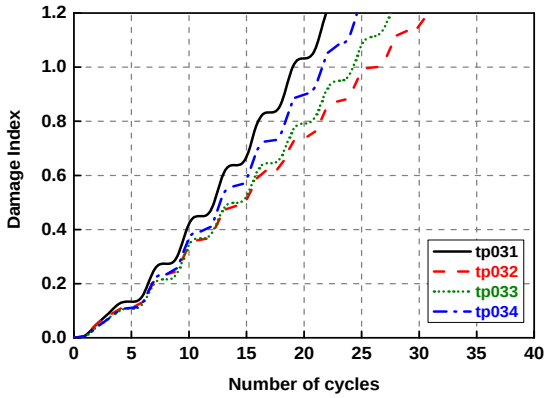

Figure 10. Progressive Damage for all specimens

5. FRAGILITY CURVES

Fragility curves express the probability of structural damage due to cyclic loading as a function of number of cycles. Based on the Park and Ang damage index data of the four tested specimens, a set of fragility curves for the bridge piers were constructed assuming a lognormal distribution

Fragility curves indicate the probability of reaching or exceeding a previously defined damage state. As previously stated, five damage states were used; these are no damage, slight, moderate, extensive and complete damage. Fig.10 shows the damage states and its values.

Once the damage index value is obtained at each cycle, the damage state is obtained following the table 4. When a damage state occurs, a 1 is written; otherwise a 0, after completing this process at each DI value for each cycle and for four models of piers, the number of occurrences is added and written.

The cumulative distribution for each damage state for the entire 4 models subjected to cyclic loading and a probability plot was created, a lognormal curve was fitted to develop a relationship between number of cycles and damage index by using least squares approach, In order to obtain the two parameters that define the lognormal distribution, the Microsoft Excel Solver tool was used.

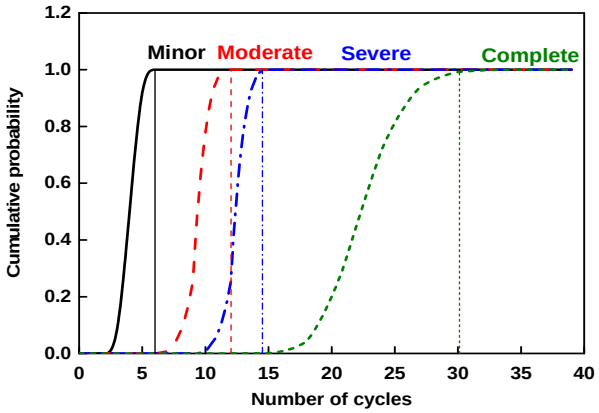

Figure 11. Fragility curves for four reinforced concrete bridge piers

Fig.11 shows the fragility curves for four reinforced concrete bridge piers. Fig.11 shows that until 6 cycles no difference in damage distribution is observed for the four specimens. Using the Park and Ang damage classification given in Table 3, it was concluded that: for no damage level the number of cycles is between (0~6) cycles; minor damage level is between (6~12) cycles; moderate damage level is between (12~14); severe damage level is between (15~30) cycles and for complete damage level is over 30 cycles.

CONCLUSIONS

In this paper some results of an analytical research program conducted to assess the seismic behavior of reinforced concrete bridge piers was presented. The analyzed specimens were chosen from the data bank of Professor Kazuhiko Kawashima. Effect axial load intensity were considered in this analysis. All specimens, in total 4, had a square cross section of 400x400mm.

It was shown the dissipated energy for specimen tp032, under a constant axial load, was constant from 3% to 6% drift which was not the case for the three other specimens. However, at 4.5% drift, the cumulative dissipated energy of specimen tp032 was only 65% of that of specimen tp033.

Numerical models for the tested specimens were developed and analyzed using SeismoStruct software. The analytical results show reasonable agreement with the experimental ones. The analysis did not only predicted the stiffness, load, and deformation at the peak with a good accuracy, but also captured the post-peak softening as well. In all cases the ratio (Qexp/Qana) was greater than 0.95 except for specimen tp032 in negative side where this value was 0.91. The mean ratios of experimental-to-analytical maximum peaks were 0.96 with a coefficient of variance (COV) of 1% for the positive side and 0.97 with a coefficient of variance (COV) of 4% for the negative side.

REFERENCES

Bae S and Bayrak O (2008) "Seismic Performance of Full-Scale Reinforced Concrete Columns", *ACI Structural Journal,* 105(2): 123-133

Chang S Y (2010) "Experimental studies of reinforced concrete bridge columns under axial load plus biaxial bending", *Journal of Structural Engineering ASCE*, 136(1):12-25

Chen Y, Feng M Q, Soyoz S (2008) "Large-Scale Shake Table Test Verification of Bridge Condition Assessment Methods", *Journal of Structural Engineering*, 7: 1235-1245

Cheok G S and Stone W C (1990) "Behavior of 1/6 scale model bridge columns subjected to inelastic cyclic loading", *ACI Structural Journal*, 87(6): 630-638

El-Bahy A, Kunnath S K, Stone W C, Taylor A W (1999a) "Cumulative seismic damage of circular bridge columns: benchmark and low-cycle fatigue tests", *ACI Structural Journal*, 96(4): 633-643

El-Bahy A, Kunnath S, Stone W, Taylor A (1999b) "Cumulative seismic damage of circular bridge columns: variable amplitude tests", *ACI Structural Journal*, 96(5): 711-719

Filippou F C, Popov E P, Bertero V V (1983) "Effects of bond deterioration on hysteretic behavior of reinforced concrete joints", Report EERC 83-19, Earthquake Engineering Research Center, University of California, Berkeley

Fujikura S, Kawashima K, Shoji G, Zhang J, Takemura H (2000) "Effect of the interlocking ties and cross ties on the dynamic strength and ductility of rectangular reinforced concrete bridge columns", *Journal of Structural Mechanics and Earthquake Engineering*, 640(I-50): 71-88

Gardoni P, Der Kiureghian A, Mosalam KM (2002) "Probabilistic models and fragility estimates for bridge components and systems", Report 2002-13, Pacific Earthquake Engineering Research Center, University of California, Berkeley

Han Q, Du X, Zhou Y, Lee G (2013) "Experimental study of hollow rectangular bridge column performance under vertical and cyclically bilateral loads", *Earthquake Engineering and Engineering Vibration*, 12(3): 433-445

Hindi RA and Sexsmith RG (2001) "A proposed damage model for RC bridge columns under cyclic loading", *Earthquake Spectra*, 17(2), 261-290

Kawashima K, Shoji G, Sakakibara Y (2000) "A cyclic loading test for clarifying the plastic hinge length of reinforced concrete Piers", *Journal of Structural Engineering*, 46A: 767-776

Mander J B, Priestley M J N, Park R (1988) "Theoretical stress strain model for confined concrete", *Journal of Structural Engineering ASCE*, 114(8): 1804-1826

Menegotto M and Pinto P (1973) "Method of analysis for cyclically loaded reinforced concrete plane frames including changes in geometry and non-elastic behavior of elements under combined normal force and bending", *Proceedings of the IABSE Symposium on Resistance and Ultimate Deformability of Structures Acted on by Well Defined Repeated Loads*, Lisbon, 15-22

Park Y J, Ang A HS (1985) "Mechanistic seismic damage model for reinforced concrete", *Journal of Structural Engineering ASCE*, 111 (4), 722-739

Park Y J, Ang A HS, Wen K (1985) "Seismic damage analysis of reinforced concrete buildings", *Journal of Structural Engineering ASCE*, 111(4), 740-757

Sakai J and Kawashima K (2002) "Effect of varying axial loads including a constant tension on seismic performance of reinforced concrete bridge piers", *Journal of Structural Engineering JSCE*, 48A: 735-746

Salawu O S and Williams C (1993) "Review of full scale dynamic testing of bridge columns", *Engineering Structures*, 17(2): 113-121

SeismoStruct (2012) a computer program for processing strong motion data 2002-2012, SeismoSoft Ltd, website www.seismosoft.com

Sheikh S A (1978) Effectiveness of rectangular ties as confinement, PhD Dissertation, University of Toronto, Canada

Sheikh S A and Toklucu M T (1993) "Reinforced concrete columns confined by circular spirals and hoops", *ACI Structural Journal*, 90(5): 542-553

Takemura H and Kawashima K (1997) "Effect of loading hysteresis on ductility capacity of reinforced concrete bridge piers", *Journal of Structural Engineering*, 43A: 849-858